Electronic Supplementary Material

Ultrasensitive H_2S gas sensors based on p-type WS_2 hybrid materials

Georgies Alene Asres[1], José J. Baldoví[2,3], Aron Dombovari[1], Topias Järvinen[1], Gabriela Simone Lorite[1], Melinda Mohl[1], Andrey Shchukarev[4], Alejandro Pérez Paz[3,5], Lede Xian[2,3], Jyri-Pekka Mikkola[4,6], Anita Lloyd Spetz[1,7], Heli Jantunen[1], Ángel Rubio[2,3] (✉), and Krisztian Kordas[1] (✉)

[1] *Microelectronics Research Unit, Faculty of Information Technology and Electrical Engineering, University of Oulu, P.O. Box 4500, FI-90014 Oulu, Finland*

[2] *Max Planck Institute for the Structure and Dynamics of Matter, Luruper Chaussee 149, 22761 Hamburg, Germany*

[3] *Nano-Bio Spectroscopy Group, European Theoretical Spectroscopy Facility (ETSF), Universidad del País Vasco, CFM SCIC-UPV/EHU-MPC DIPC, Avenida Tolosa 72, 20018 San Sebastian, Spain*

[4] *Technical Chemistry, Department of Chemistry, Chemical-Biological Centre, Umeå University, SE-90187 Umeå, Sweden*

[5] *School of Chemical Sciences and Engineering, School of Physics and Nanotechnology, Yachay Tech University, Urcuquí, Ecuador*

[6] *Industrial Chemistry & Reaction Engineering, Department of Chemical Engineering, Johan Gadolin Process Chemistry Centre, Åbo Akademi University, FI-20500 Åbo-Turku, Finland*

[7] *Sensor and Actuator Systems, Department of Physics, Chemistry and Biology, Linköping University, SE-58183 Linköping, Sweden*

Supporting information to https://doi.org/10.1007/s12274-018-2009-9

Resistive and field-effect transistor H_2S sensors

Table S1 Resistive and field-effect transistor H_2S sensors and their properties reported in the literature

Method	Sensing material	Sensitivity[a]	Operating temperature	Lowest experimental H_2S concentration[b]	Ref.
Resistive	WS_2 nanowire-nanoflake hybrid	0.043 ppm^{-1}	200 ºC	0.02 ppm	This work
Resistive	α-Fe_2O_3 nanoparticles	~5.2 ppm^{-1}	300 ºC	0.05 ppm	[1]
Resistive	CuO nanosheets	~3.3 ppm^{-1}	240 ºC	0.03 ppm	[2]
Resistive	Mesoporous WO_3	~50 ppm^{-1}	250 ºC	0.25 ppm	[3]
Resistive	CeO_2 nanowire	~2 ppm^{-1}	Room temp.	0.05 ppm	[4]
Resistive	PbS quantum dots	~140 ppm^{-1}	135 ºC	10 ppm	[5]
Resistive	ZnO nanostructures	~0.14 ppm^{-1}	300 ºC	20 ppm	[6]
Resistive	Pt-loaded WO_3 thin films	~1200 ppm^{-1}	100 ºC	1 ppm	[7]
Resistive	Nanocrystalline In_2O_3-SnO_2	~20 ppm^{-1}	40 ºC	2 ppm	[8]
Resistive	SnO_2 thin film	0.2 ppm^{-1}	300 ºC	5 ppm	[9]
Resistive	SnO_2 nanocolumns	2.8 ppm^{-1}	300 ºC	5 ppm	[9]
Resistive	SnO_2 nanocolumns decorated with Au	22 ppm^{-1}	300 ºC	5 ppm	[9]
Resistive	SnO_2 nanocolumns decorated with Ag	12.8 ppm^{-1}	300 ºC	5 ppm	[9]
FET	Ultrathin Ph5T2 microplates	240 ppm^{-1}	Room temp.	0.5 ppm	[10]
FET	CuPc	0.004 ppm^{-1}	Room temp.	100 ppm	[11]
FET	In_2O_3 nanowires	0.41 ppm^{-1}	Room temp.	1 ppm	[12]

[a] The highest sensitivity values are calculated from the published references as the relative change of electrical resistance normalized to the corresponding H_2S concentration i.e. $\Delta R/(R_0 \cdot C_{H2S})$. When the electrical current values were reported, the sensitivity values were calculated from the relative change of the current at the corresponding gas concentration, i.e. $\Delta I/(I_0 \cdot C_{H2S})$.

Address correspondence to Krisztian Kordas, krisztian.kordas@oulu.fi; Angel Rubio, angel.rubio@mpsd.mpg.de

Theoretical calculations

Adsorption energy and equilibrium height

For the study of the adsorption of H_2S upon WS_2 monolayer, we considered four adsorption sites: the center of a hexagon (H), the center of a W–S bond (B), the top of a W atom (TW) and the top of a S atom (TS) (Figure S1). For each anchoring site we investigated three possible orientations of the H_2S molecule, namely *up* (the H atoms pointing away from the surface), *down* (the H atoms pointing towards the slab) and *par* (the bonds H–S parallel to the monolayer).

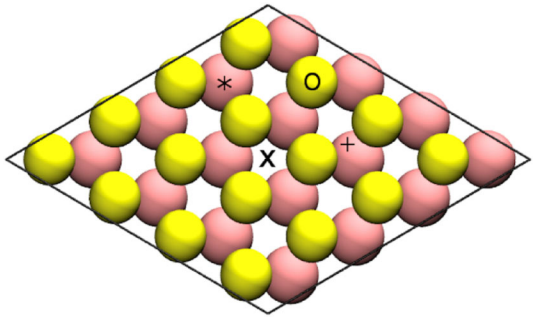

Figure S1 4x4 supercell of the relaxed pristine monolayer WS_2. The four adsorption sites are labelled as H (X), B (+), TW (*) and TS (o).

For each geometrical optimization of the system (supercell+molecule) we calculated the total energy. The total energies of the H_2S molecule and the clean slab supercell using the same unit cell were -310.05 and -38668.53 eV respectively. The calculated adsorption energy (E_{ads}) and the equilibrium height (h) for each case are reported in Table S2.

Table S2 Calculated adsorption energy (E_{ads}) and equilibrium height for the different adsorption sites of H_2S molecule on pristine WS_2 monolayer.

	E_{ads} / meV	h / Å
H_{up}	-156.509	3.33
H_{down}	**-181.365**	2.55
H_{par}	-177.500	2.66
B_{up}	-172.414	2.97
B_{down}	-169.677	2.59
B_{par}	-150.301	2.72
TW_{up}	-153.173	3.36
TW_{down}	**-181.106**	2.56
TW_{par}	-172.040	2.62
TS_{up}	-109.107	3.63
TS_{down}	-146.507	2.79
TS_{par}	-164.308	2.76

As can be observed in Table S2 there are two anchoring positions that show a more marked stability. These are the H and TW sites with adsorption energy of ~ -181 meV. However, we could not appreciate significant differences between the determined electronic structures in both more stable sites, which allowed us to perform all the calculations from the H anchoring position in order to simulate the interaction of H_2S with the hybrid

material. Subsequently, we have structurally optimized the adsorption of H_2, CO, NO and NH_3 upon the WS_2 supercell. As a starting point, we placed the gas molecules in the most stable orientation determined using LDA [13], i.e. TW, H, B and H respectively. The most favorable configurations according to our results are reported in Figures S2-S5.

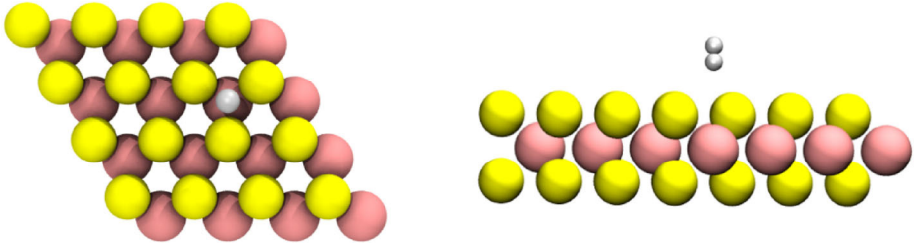

Figure S2 Relaxed geometries for H_2 adsorbed on pristine monolayer WS_2. (left) Top and (right) side view of the most favorable DFT/PBE-D2 relaxed geometries for H_2 adsorbed on pristine monolayer WS_2. The S, W and H atoms are depicted by the yellow, pink and white spheres, respectively.

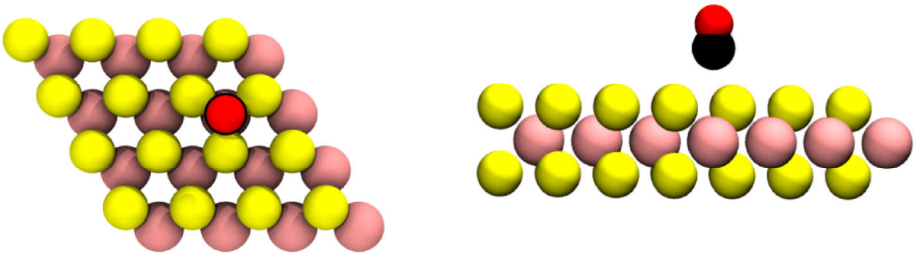

Figure S3 Relaxed geometries for CO adsorbed on pristine monolayer WS_2. (left) Top and (right) side view of the most favorable DFT/PBE-D2 relaxed geometries for CO adsorbed on pristine monolayer WS_2. The S, W, C and O atoms are depicted by the yellow, pink, black and red spheres, respectively.

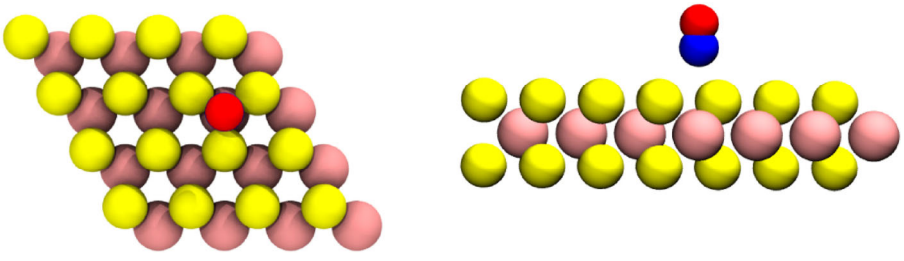

Figure S4 Relaxed geometries for NO adsorbed on pristine monolayer WS_2. (left) Top and (right) side view of the most favorable DFT/PBE-D2 relaxed geometries for NO adsorbed on pristine monolayer WS_2. The S, W, N and O atoms are depicted by the yellow, pink, blue and red spheres, respectively.

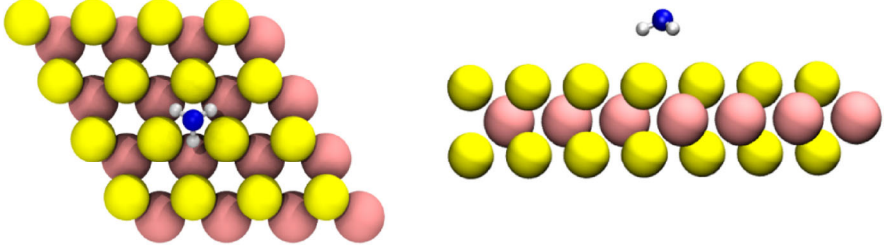

Figure S5 Relaxed geometries for NH_3 adsorbed on pristine monolayer WS_2. (left) Top and (right) side view of the most favorable DFT/PBE-D2 relaxed geometries for NH_3 adsorbed on pristine monolayer WS_2. The S, W, N and H atoms are depicted by the yellow, pink, blue and white spheres, respectively.

The adsorption energies are -57.4 meV (H_2), -84.7 meV (CO), -509.3 meV (NO) and -171.7 meV (NH_3). The calculated E_{ads} are in good qualitative agreement with the ones calculated within LDA: -75 meV (H_2), -127 meV (CO), -206 meV (NO) and -216 meV (NH_3) [13]. The exception is the case of NO, which we properly describe using spin-polarized calculations, whereas LDA results for NO [13] were incorrectly calculated at the spin-paired level. On the other hand, if we compare quantitatively, one can observe the smaller binding energy for all the studied gases determined within GGA+vdW, which is consistent with the general trend towards underbinding (overbinding) typical of GGA(LDA) [14].

Electronic structure

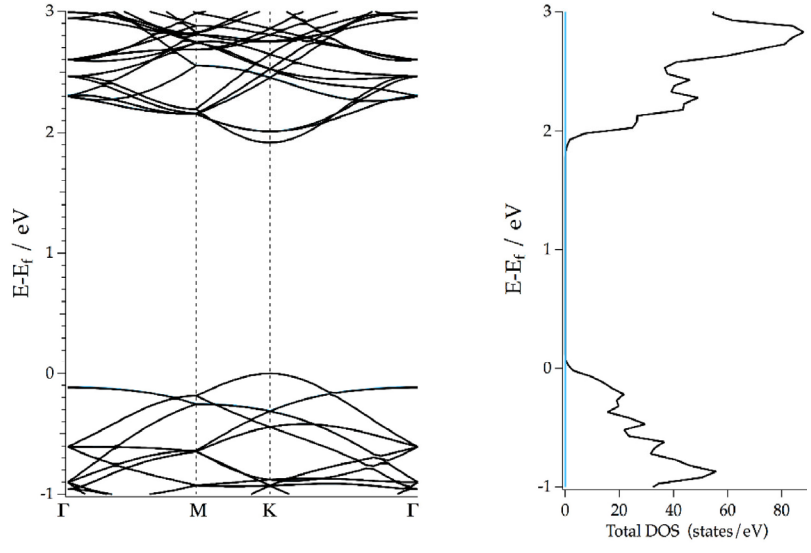

Figure S6 Calculated electronic band structure and density of states of H_2 adsorbed on monolayer WS_2. The sky blue line represent the projection of the local density of states of the H_2 gas molecule.

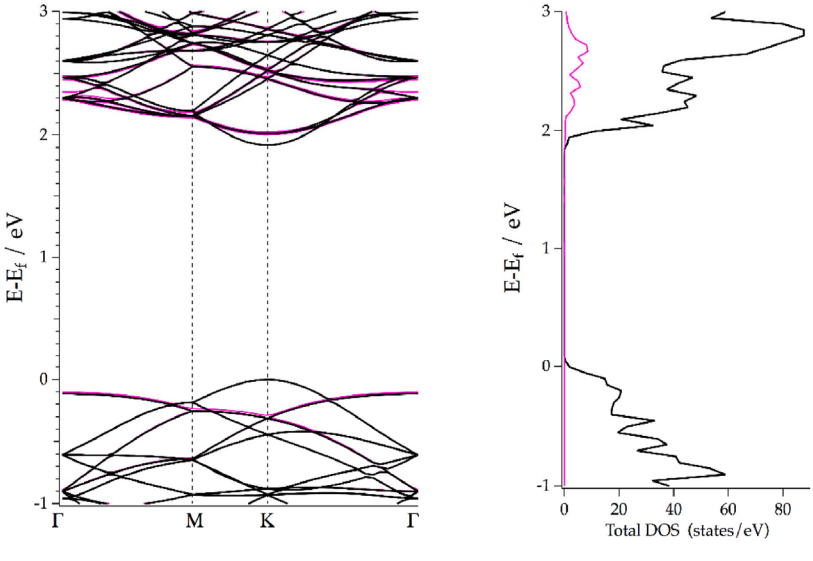

Figure S7 Calculated electronic band structure and density of states of CO adsorbed on monolayer WS_2. The pink line represent the projection of the local density of states of the CO gas molecule.

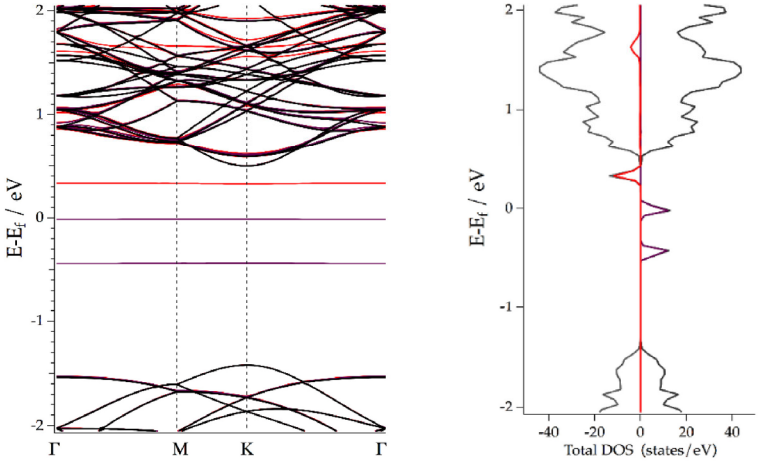

Figure S8 Calculated electronic band structure and density of states of NO adsorbed on monolayer WS_2. The red (spin up) and purple (spin down) lines represent the projection of the local density of states of the NO gas molecule.

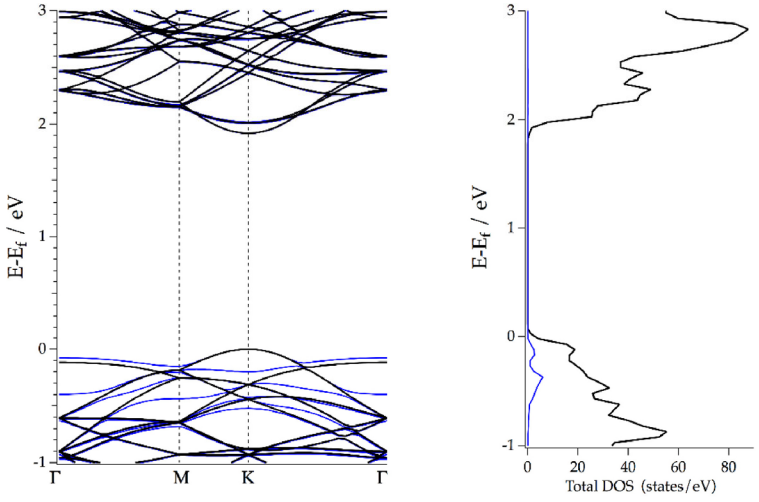

Figure S9 Calculated electronic band structure and density of states of NH_3 adsorbed on monolayer WS_2. The blue line represent the projection of the local density of states of the NH_3 gas molecule.

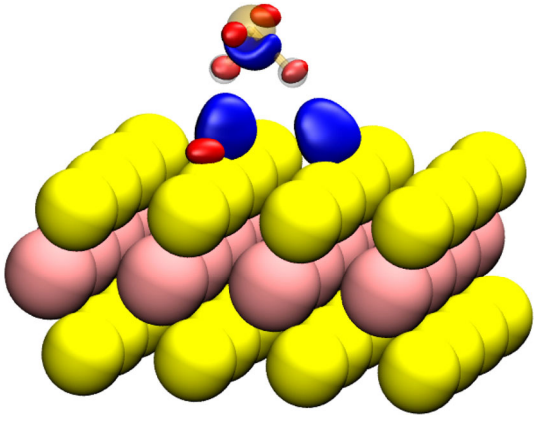

Figure S10 Valence electronic density differential plot with an isosurface value of 0.0004 e/Bohr^3. Blue (red) depicts electron accumulation (depletion) regions, respectively. Reorganization of the electronic density in H_2S molecule upon adsorption and electron accumulation at the interface are visible. However, this density redistribution is small in absolute terms and moreover Bader charge analysis predicts no net electron transfer between H_2S and WS_2 slab.

Table S3 Comparison of the calculated charge transfer from PBE-D2 and LDA for the different gas species adsorbed on pristine monolayer WS_2. Positive values mean transfer from WS_2 to adsorbate.".

Gas	GGA - This work	LDA [13]
H_2	0.004	0.002
CO	0.003	0.022
NO	0.008	0.018
NH_3	-0.017	-0.061
H_2S	0.005	–
H_2S (bilayer)	0.002	–

References

[1] Li, Z.; Huang, Y.; Zhang, S.; Chen, W.; Kuang, Z.; Ao, D.; .Liu, W.; Fu, Y. A fast response & recovery H_2S gas sensor based on α-Fe_2O_3 nanoparticles with ppb level detection limit. *J. Hazard. Mater.* **2015**, *300*, 167-174.

[2] Zhang, F., Zhu, A., Luo, Y., Tian, Y., Yang, J.; Qin, Y. CuO nanosheets for sensitive and selective determination of H_2S with high recovery ability. *J. Phys. Chem. C*, **2010**, *114*, 19214-19219.

[3] Li, Y.; Luo, W.; Qin, N.; Dong, J.; Wei, J.; Li, W.; Feng, S.; Chen, J.; Xu, J.;Elzatahry, A.A.; Es-Saheb, M.H.; Deng, Y.; Zhao, D. Highly ordered mesoporous tungsten oxides with a large pore size and crystalline framework for H_2S sensing. *Angew. Chem.* **2014**, *53*, 9035-9040.

[4] Li, Z.; Niu, X.; Lin, Z.; Wang, N.; Shen, H.; Liu, W.; Sun, K.; Fu, Y.Q.; Wang, Z. Hydrothermally synthesized CeO_2 nanowires for H_2S sensing at room temperature. *J. Alloy. Comp.*, **2016**, *682*, 647-653.

[5] Li, M.; Zhou, D.; Zhao, J.; Zheng, Z.; He, J.; Hu, L.; Xia, Z.; Tang, J.; Liu, H. Resistive gas sensors based on colloidal quantum dot (CQD) solids for hydrogen sulfide detection. *Sens. Actuat. B*, **2015**, *217*, 198-201.

[6] Mortezaali, A.; Moradi, R. The correlation between the substrate temperature and morphological ZnO nanostructures for H_2S gas sensors. *Sens. Actuat. A*, **2014**, *206*, 30-34.

[7] Shen, Y.; Zhang, B.; Cao, X.; Wei, D.; Ma, J.; Jia, L.; Gao, S.;Cui, B.; Jin, Y. Microstructure and enhanced H_2S sensing properties of Pt-loaded WO_3 thin films. *Sens. Actuat. B*, **2014**, *193*, 273-279.

[8] Liu, H.; Wu, S.; Gong, S.; Zhao, J.; Liu, J.; Zhou, D. Nanocrystalline In_2O_3–SnO_2 thick films for low-temperature hydrogen sulfide detection. *Ceram. Int.*, **2011**, *37*, 1889-1894.

[9] Yoo, K. S.; Han, S. D.; Moon, H. G.; Yoon, S. J.; Kang, C. Y. Highly sensitive H_2S sensor based on the metal-catalyzed SnO_2 nanocolumns fabricated by glancing angle deposition. *Sens.* **2015**, *15*, 15468-15477.

[10] Zhao, X.; Tong, Y.; Tang, Q.; Tian, H.; Liu, Y. Highly sensitive H_2S sensors based on ultrathin organic single-crystal microplate transistors. *Org. Electron.*, **2016**, *32*, 94-99.

[11] Li, X.; Jiang, Y.; Xie, G.; Tai, H.; Sun, P.; Zhang, B. Copper phthalocyanine thin film transistors for hydrogen sulfide detection. *Sens. Actuat. B* **2013**, *176*, 1191-1196.

[12] Zeng, Z.; Wang, K.; Zhang, Z.; Chen, J.; Zhou, W. The detection of H_2S at room temperature by using individual indium oxide nanowire transistors, *Nanotechnol*. **2009**, *20*, 045503.

[13] Zhou, C.; Yang, W.; Zhu, H.; Mechanism of charge transfer and its impacts on Fermi-level pinning for gas molecules adsorbed on monolayer WS_2. *J. Chem. Phys.*, **2015**, *142*, 214704.

[14] Simeoni, M.; Picozzi, S.; Delley, B. An ab-initio study of pentacene on aluminum (100) surface. *Surf. Sci.* **2004**, *562*, 43–52.